Evaluation of Boundary-Layer and Parabolized Navier-Stokes Solutions for Re-entry Vehicles

Mary McWherter,* Ralph W. Noack,* and William L. Oberkampf†
Sandia National Laboratories, Albuquerque, New Mexico

Numerical predictions made by a traditional inviscid/boundary-layer method and a parabolized Navier-Stokes method are compared with wind tunnel data for slender, blunted cones at moderate angle of attack. Mach numbers ranged from 6 to 14 and Reynolds numbers from 0.4 to 16 million. The purpose of the comparison is to evaluate the Mach number and Reynolds number range of applicability of the two prediction methods. Also described are the practical aspects of using these two methods in a design environment.

Nomenclature

A_b = base area
C_∞ = form of Chapman-Rubesin viscosity coefficient, $(\mu_w/\mu_\infty)(T_\infty/T_w)$
C_a = forebody axial force coefficient, $(F_A/q_\infty A_b)$, based on $p_b = p_\infty$
C_m = pitch moment coefficient, $(M/q_\infty A_b D_b)$, taken about the base
C_n = normal force coefficient, $(F_N/q_\infty A_b)$
D_n = nose diameter
D_b = base diameter
DS = normal direction step size in PNS code
DX = axial step size in PNS code
e = total energy per unit volume
E,F,G = inviscid flux vectors in the governing equations
F_A = axial force
F_N = normal force
J = Jacobian of the transformation
L = vehicle length
M = pitch moment
M_∞ = freestream Mach number
p = static pressure
p_∞ = freestream static pressure
p_b = base pressure
PER = fraction of radial grid points to be clustered
q_∞ = freestream dynamic pressure
R,S,T = viscous flux vectors in the governing equations
R_{∞_L} = Reynolds number based on vehicle length, $(\rho_\infty V_\infty L/\mu_\infty)$
T_∞ = freestream static temperature
T_0 = freestream stagnation temperature
T_w = model wall temperature
u,v,w = Cartesian velocity components
$\bar{v}_\infty$ = hypersonic viscous interaction parameter, $M_\infty[C_\infty/R_{\infty_L}]^{1/2}$
x_{cp}/L = normalized center of pressure in x, measured from the nose
x,y,z = Cartesian coordinates
ξ,η,ζ = Generalized coordinates of computation space
ρ = mass density
ϕ = circumferential angle from windward
μ = absolute viscosity

Subscripts

x,y,z = partial derivatives in x,y,z directions, respectively
ξ,η,ζ = partial derivatives in ξ,η,ζ directions, respectively

Presented as Paper 84-0486 at the AIAA 22nd Aerospace Sciences Meeting, Reno, NV, Jan. 9-12, 1984; submitted Dec. 20, 1984; revision submitted May 31, 1985.

*Member Technical Staff. Member AIAA.
†Member Technical Staff. Associate Fellow AIAA.

Introduction

MODERN techniques for estimating aerodynamic performance of re-entry vehicles are based on solving the inviscid flow and shock equations using finite-difference methods.[1-5] For performance characteristics which require the viscous contribution, the inviscid flow solution is used to calculate a boundary-layer solution.[6,7] This approach is highly developed and provides accurate design estimates over a wide range of Mach and Reynolds number.

The relatively new parabolized Navier-Stokes approach for calculating hypersonic, viscous flowfields has received considerable attention in the last ten years.[8-19] Shock layers dominated by locally supersonic flows are often well represented by conservation equations containing the parabolized Navier-Stokes (PNS) approximations. The PNS approximations remain valid in regions of strong viscous-inviscid interaction, where weak interaction approaches, such as the inviscid/boundary-layer theory, are no longer valid. Even though this is understood by the design engineer, he or she must balance the accuracy of each approach with the equally important practical aspects of ease of use, robustness, and the computer time required.

In this paper, surface pressure and force and moment predictions from the inviscid/boundary-layer and PNS methods are compared with wind tunnel data. These theory and experiment comparisons are made over the range of Mach numbers 6 to 14 and Reynolds numbers (based on length) from 0.4×10^6 to 16×10^6. At Mach 6 and high Reynolds number, a weak viscous-inviscid interaction flow field is expected. At Mach 14 and low Reynolds number, however, a much stronger viscous-inviscid interaction should appear. With this wide range of Mach and Reynolds numbers, it can be determined where the assumptions of weak interaction theory begin to break down and a strong interaction method, such as the PNS approach, is required. The purpose of this paper is two-fold: first, to evaluate the accuracy of both methods over a wide range of Mach and Reynolds numbers, and second, to briefly describe the numerical and practical considerations in using both solution methods in a design environment.

Description of Solution Techniques

Inviscid/Boundary-Layer Solution

The inviscid/boundary-layer solution technique used here assumes that the viscous region of the flowfield has no effect on the inviscid portion of the flowfield. The inviscid

flowfield about the body is first obtained, and then a boundary-layer solution is calculated for the inviscid pressure distribution and streamlines. The inviscid pressure distribution can then be modified by a simple, approximate method to account for the displacement effect of the boundary layer.

The inviscid/boundary-layer solution technique currently in use at Sandia was developed by the General Electric Company: the GE Flow Field System (GEFFS).[5,7] The GEFFS consists of a three-dimensional inviscid flowfield code (3IFF) and a three-dimensional boundary-layer code (3DV).

Inviscid Solution

The 3IFF code contains a two- and a three-dimensional transonic nosetip code and an afterbody code. The Euler equations with velocity components, entropy, and the logarithm of pressure as the dependent variables are the governing equations solved in 3IFF. The nosetip codes solve the unsteady, nonconservative form of the equations and the afterbody portion of 3IFF solves the supersonic, spatially marching form of the nonconservative (or the weakly conservative) equations.

The inviscid flowfield is solved between the bow shock and the body in the nose and afterbody regions. Explicit type boundary conditions are applied at the body and the bow shock surface. The body boundary conditions utilize a method of characteristics technique to predict the body surface pressure. Although the surface entropy is a constant in inviscid flow, an entropy relaxation technique is used to better simulate the real viscous flowfield and remove the strong entropy gradients which can result from the blunt body entropy layer. Flow tangency is the final boundary condition at the body surface. The bow shock surface is tracked using a method based on the method of characteristics. Once the bow shock location and orientation is known, flow properties behind the shock are determined from the Rankine-Hugoniot shock relations.

The blunt body solution is used as the starting condition for the after-body solution. Simple radial type grids are constructed between the body and the shock for the blunt body and the afterbody solutions. This grid is transformed to a rectangular computational domain using a simple shearing transform. The explicit McCormack scheme is used to solve the finite-difference form of the governing equations.

Boundary-Layer Solution

The boundary-layer code 3DV solves integral boundary-layer equations along inviscid streamlines. The surface pressure distribution is obtained from the inviscid code 3IFF. This surface pressure is used as the forcing function for the boundary-layer equations and is used in the location of the inviscid streamlines.

The inviscid streamline paths are determined using the method of DeJarnette. This method integrates the axial and circumferential momentum equations with the surface pressure gradients given.

The 3DV code solves the integral form of the momentum and energy boundary-layer equations. These equations have been derived in a streamwise coordinate system assuming small cross-flow. Laminar boundary layers is calculated with a quartic polynomial velocity profile; a power law profile is used for the turbulent case. An exponent of 1/7 is normally used in the turbulent profile.

The 3DV code includes the effects of equilibrium real gas, entropy swallowing, pressure gradient, and surface mass addition. The effects of angle of attack are accounted for by including the effects of local property variations, streamline spreading, and changes in boundary-layer profile derivatives at the wall. The code calculates skin friction, heat transfer, and an induced pressure.

The induced pressure is used to approximate the effect the boundary-layer displacement thickness has upon the inviscid surface pressure. The Sandia version of 3DV uses linear-supersonic flow theory and the change in surface slope due to displacement thickness to estimate the induced pressure. It is implicit in all future references to the 3DV code that the 3IFF inviscid solution was used to provide the surface pressure distribution and bow shock shape.

Parabolized Navier-Stokes Solution

The Air Force Wright Aeronautical Laboratory (AFWAL) Parabolized Navier-Stokes (PNS) code, currently used at Sandia, is based upon the numerical work of Schiff and Steger[15] and others.[16-19] In order to start the PNS code, two initial planes of supersonic flow data are required. The NASA Ames thin-layer Navier-Stokes code[20-22] is used to compute the flowfield around the nose. The afterbody portion is then solved using the AFWAL PNS code.

Formulation of the Flowfield Equations

The three-dimensional, steady, Navier-Stokes equations are arranged in strong conservation-law form for nondimensional Cartesian spatial variables, x, y, and z. Transforming to body conforming coordinates, three independent spatial variables are introduced. These variables transform the physical x, y, z space surrounding the body into a rectangular ξ,η,ζ computational domain.

In the work done by Schiff and Steger[15] the transformation is of the form

$\xi=\xi(x)$	streamwise coordinate
$\eta=\eta(x,y,z)$	circumferential coordinate
$\zeta=\zeta(x,y,z)$	normal coordinate

For hypersonic flow problems, the shock layer is mapped such that the body surface is the plane $\zeta=0$ and the bow shock is the plane $\zeta=\zeta_{\max}$. This transformation simplifies the application of surface and shock boundary conditions and helps make possible both the thin layer approximation and the PNS approximation in the subsonic layer.

The strong conservation-law form can be preserved in the ξ,η,ζ transformation of coordinates by retaining the Cartesian velocity components as dependent variables. The transformed equations become

$$\frac{\partial\hat{E}}{\partial\xi}+\frac{\partial\hat{F}}{\partial\eta}+\frac{\partial\hat{G}}{\partial\zeta}=\frac{1}{R_{\infty L}}\left(\frac{\partial\hat{R}}{\partial\xi}+\frac{\partial\hat{T}}{\partial\eta}+\frac{\partial\hat{S}}{\partial\zeta}\right) \tag{1}$$

where

$$\hat{E}=\frac{\xi_x}{J}E$$

$$\hat{F}=\frac{\eta_x}{J}E+\frac{\eta_y}{J}F+\frac{\eta_z}{J}G$$

$$\hat{G}=\frac{\zeta_x}{J}E+\frac{\zeta_y}{J}F+\frac{\zeta_z}{J}G$$

and

$$J^{-1}=x_\xi(y_\eta z_\zeta-y_\zeta z_\eta)$$

PNS Approximations

The PNS equations are obtained from Eq. (1) by neglecting the streamwise viscous diffusion terms and by modifying the convective flux vector to permit stable time-like marching of the equations downstream from initial data. The latter assumption restricts the flow so that flow separation in the streamwise direction, for example, near a large flap deflection, is not allowed, while cross-flow separation is permitted. It is not necessary to drop the circumferential

derivatives $\partial\eta$, but doing so does simplify the computations and is, therefore, incorporated into the development of the equations. These approximations are physically justified for high to moderate Reynolds number flow past bodies with mild axial geometry changes. The resulting set of equations include the continuity equation, three momentum equations, and the energy equation written in matrix form as

$$\frac{\partial \hat{E}}{\partial \xi}+\frac{\partial \hat{F}}{\partial \eta}+\frac{\partial \hat{G}}{\partial \zeta}=\frac{1}{R_{\infty L}}\left(\frac{\partial \hat{S}}{\partial \zeta}\right) \tag{2}$$

where the Stokes hypothesis is used to obtain the viscous terms. The equations are elliptic in the circumferential and radial directions, and parabolic with respect to the downstream marching coordinate. For turbulent flow computations, the eddy-viscosity model described by Baldwin and Lomax[23] is employed.

The treatment of the streamwise pressure gradient term $\partial p/\partial \xi$ in the subsonic layer is the crucial approximation in PNS methods. In the approach developed by Rubin and Lin,[24] $\partial p/\partial \xi$ from the adjacent supersonic flow is impressed down through the thin viscous subsonic layer. This approach is similar, in concept, to classical boundary-layer concepts. However, in this approach the constant pressure region includes only the subsonic part of the viscous region, and the imposed pressure is meant to be calculated concurrently with the calculation of the entire plane.

Numerical Algorithm

The PNS equations are formulated into an approximately factored, locally linearized form. The algorithm is a noniterative, implicit, finite-difference algorithm. It is in conservative form and is second-order accurate in the marching and transverse directions. Solutions are obtainable for flow which is inviscid or viscous, either laminar or turbulent. A fairly complete description of the solution procedure is given in Ref. 19.

Four smoothing and stabilizing terms have been included in the numerical formulation. The smoothing terms are meant to damp the high frequency oscillations often associated with centered difference formulations. The stabilizing terms are used to insure that terms along the main diagonal of the streamwise matrix Jacobian are nonzero in the sublayer. These terms will be further discussed in the next section.

Obtaining a Starting Solution

The NASA Ames blunt body code[22] determines the three-dimensional flow over generalized nosetips using an unsteady implicit algorithm which solves the thin layer Navier-Stokes equations. The thin layer model is valid only for high to moderate Reynolds number flows. The equations are solved by inverting block tridiagonal systems in each space coordinate direction and marching in time until a steady-state solution is reached.

As the blunt body solution is obtained over a sphere, the flowfield can simply be rotated for angle-of-attack cases over an axisymmetric afterbody. A preprocessor program takes the blunt body solution and matches the spherical nose to the conical afterbody. It then interpolates to determine the flow at two axial stations: one at the sphere-cone tangency point and the other at one axial step upstream. The grid is then reclustered to match the PNS code requirements.

Use of Solution Techniques

3DV Solutions

The 3DV codes consist of a set of overlayed inviscid codes (to obtain the nosetip and afterbody solutions) and a boundary-layer code. These codes have been modified to fit into a production type environment and are very easy to run. Thus, for a simple geometry such as a spherically capped cone, no user interaction is required to adjust damping parameters or step size. Generating solutions for high angle-of-attack conditions can be accomplished as quickly as those for low angles of attack. An interactive preprocessor has been written at Sandia to generate the necessary control and data stream to run the 3DV codes. This interactive processor allows the user to generate within a few minutes the hundreds of runs which might be required to provide the aerodynamic data for a trajectory optimization.

This type of use of the 3DV flowfield code is practical due to low user interaction requirements and low computer time requirements. Each case presented here required approximately 10 s of execution time on a CYBER-76 computer for the inviscid solution and less than 20 s for the boundary-layer solution. These low execution times allow job turnaround times on the order of minutes to an hour on a busy computer. This type of turnaround is required to meet the demand of rapid response to production and exploratory concept requests.

PNS Solutions

Obtaining a PNS solution requires careful selection of input parameters. As the code is currently used, there are several input parameters which the user may vary slightly and still obtain a solution. Typically, improper choice of these parameters can yield unstable solutions, but they do not have a large affect on accuracy. In our experiences with the code, we have been able to arrive at some conclusions about the values to be used for some of the input parameters and the effects of these values on stability and accuracy.

Axial Step Size

Probably the most important input parameter affecting stability is the axial step size DX. If the initial step size is too small, the solution will have surface pressure oscillations in the marching direction and possibly diverge. A good method of estimating the minimum initial axial step size is to determine the physical distance from the surface to the sonic line. This suggestion is based on the work done by Rubin[32] who, for stability reasons, suggested that a minimum marching step size should be proportional to the thickness of the subsonic layer.

It has been found that a maximum value for DX is harder to determine. If DX is too large initially, large flow gradients along the body, such as, near the nose on a hemisphere-cone, cannot be properly resolved. Once the code has marched away from the nose bluntness effects, there are typically no large axial gradients, and a large DX should yield an accurate solution. A large DX will also greatly decrease the computation time on long slender re-entry vehicle configurations.

To resolve the initial flow gradients and still have a large step size farther down the body, the step size is allowed to gradually increase as the code marches down the body. In this way, the code can start with a small value for DX to resolve the initial gradients and then use a larger value farther down the body where the axial flow gradients are small for the geometry of interest here.

Radial Step Size

The spacing in the normal direction at the body surface is determined by the input parameters DS. This parameter is the distance from the body surface to the first grid point as a percentage of the distance to the bow shock. For angle-of-attack cases, the physical distance of the first grid point from the body will vary around the body as the shock standoff distance varies circumferentially.

The value of DS directly affects the number of points in the subsonic layer. If DS is too small, there will be too many points in the subsonic layer and the solution may be

numerically unstable. In the documentation for the AFWAL PNS code,[19] it is suggested that one use a maximum of seven or eight points below the sonic line for stability and accuracy.

Smoothing and Stabilizing Parameters

Another important input parameter is the coefficient of the explicit damping term, ϵ_e. The explicit smoothing term is proportional to fourth-order differences in both the circumferential and normal directions and is added to the right-hand side of the equations in numerical form. The user is able to control the size of the smoothing term by means of the constant ϵ_e. The value chosen for ϵ_e must be large enough so that oscillations in the shock shape do not occur. If ϵ_e is too large, however, nonphysical results will appear in the solution. If DX grows, ϵ_e also grows because it is scaled by DX in the numerical formulation.

An implicit smoothing parameter, ϵ_i is included on the left side of the factored numerical equations. It was initially introduced to maintain stability when large values of ϵ_e are required to damp high frequency oscillations. Stable calculations will be maintained for any positive value of ϵ_e as long as ϵ_i is at least twice the value of ϵ_e.

Two other input constants, ϵ_a and ϵ_b are included for stability. The parameter ϵ_a is added to the difference equations to insure that the entire primary diagonal of the block tridiagonal never goes to zero. The parameter ϵ_a is meant to cause the smoothing terms to increase or decrease in size as the grid changes radially and circumferentially. Since excessive values of the stabilizing damping terms lead to nonphysical terms in the equations, ϵ_a and ϵ_b are assigned values of 0.05 or 0.1, depending upon the problem and not allowed to increase axially. In cases of high angle of attack, larger values of smoothing parameters are generally required to obtain a stable solution.

Fraction of Grid Clustering

The fraction of shock-layer grid points to be clustered in the normal direction near the body surface is determined by the input parameter PER. PER is the fraction of the number of points normal to the surface from the body to the shock which will be clustered. The radial spacing will grow exponentially for a fraction of PER points and then smoothly attain the constant value used for the remainder of points.

A study of the effect of PER on the flowfield grid was made for values of 0.4 to 0.9. It was determined that values in the 0.4 to 0.6 range yield a good cross-flow plane grid. Values greater than 0.6 caused the grid to be too coarse in the outer region near the shock. This caused poor resolution of the flow in this area and typically caused static pressure distributions in the cross-flow plane to be quite erratic. The value of 0.6 has been used for all of the solutions presented here.

Computing Time

The most computer intensive part of obtaining a PNS solution is solving the blunt nose portion. The NASA Ames Blunt Body Code currently in use at Sandia requires from 20 to 30 min on the Cray 1S computer to converge to a solution. If an already converged solution is available and it is near the desired Mach number and Reynolds number, a new solution can be obtained in 5 to 15 min. A significant savings in computer time could be gained if one were to calculate blunt body solutions using a hypersonic viscous shock-layer technique.

Preparing the blunt-body solution for the PNS code in the preprocessor requires roughly 30 s on a Cyber 76 computer. The preprocessor program can be used to determine the distance to the sonic line, which fundamentally affects the proper choice of input parameters DX and DS. The PNS code itself takes about 1.7 s per step, or, usually, 5 to 10 min on the Cyber 76. As the PNS code takes relatively long to obtain a solution, it is particularly efficient to use the preprocessor to determine whether or not DX and DS have their proper values. Thus, the amount of computing time is kept to a minimum.

Typical computer times for the present sphere-cone solutions were: 4 min for the Mach 5.95 cases, 8 min for the Mach 14.1 cases, while the remainder of the cases fell within these values. For the present blunt cones, an algebraic grid generator was used which constructed the grid radially from the body to the shock and evenly distributed the circumferential points. The grid consisted of 46 circumferential points and 30 points radially. For more difficult configurations such as a wing-body, a hyperbolic grid generator is used which constructs a grid normal to the body at the surface and allows circumferential clustering. The run times using the hyperbolic grid generator are typically 2.5 s per axial step.

Results

In order to determine the accuracy and range of applicability of each solution procedure, comparisons with available experimental data are presented for slender sphere-cones at low to moderate angles of attack. The comparisons cover a wide range of Mach and Reynolds numbers in order to evaluate each procedure for cases where there is strong viscous-inviscid interaction. In this way, it can be determined when the inviscid/boundary-layer solution is no longer valid and a PNS type solution is needed. The comparisons are presented for surface pressure data and force and moment data for Mach numbers from 6 to 14. More extensive comparisons of both solution techniques with experiment are given in Ref. 33.

Mach 6 Comparisons

Figures 1 through 3 show the results at Mach 5.95 for a 6 deg half-angle cone. As the Reynolds number (based on model length) for this case was 15.2 million, the PNS and 3DV calculations assumed a turbulent boundary layer. The surface pressure measurements were for a sphere-cone with a 2.01 in. nose diameter and a length of 38.91 in. The force

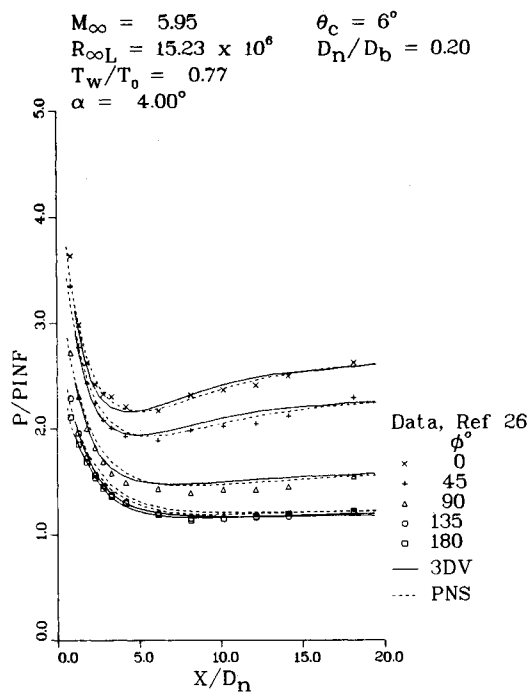

Fig. 1 Surface pressure vs axial distance for Mach 6 at $\alpha = 4$ deg.

and moment measurements were taken from a different model, which had a 1.5-in. nose diameter and a length of 41.5 in.

In Figs. 1 and 2, results from the two methods are compared to experimental surface pressures measurements for angles of attack of 4 and 8 degs. Each figure shows the axial distribution of surface pressure for 45 deg increments from the windward side to the leeward side. Both methods provide good agreement with the experimental data for 4 deg angle of attack. For 8 deg angle of attack, the 3DV prediction overestimates the pressure on the 45 and 90 deg rays over most of the body length. It should be pointed out that the inviscid flow prediction of pressure on the 45 and 90 deg rays is almost identical to the PNS prediction. This implies that the induced pressure calculation overestimates the effect of the boundary-layer displacement thickness on surface pressure in certain situations.

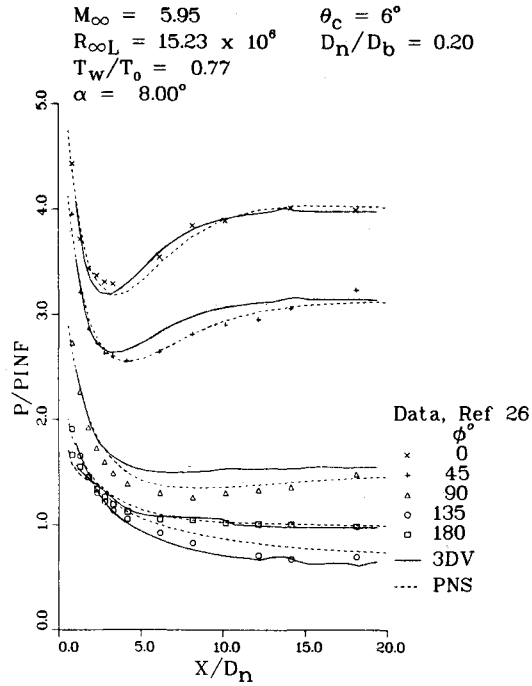

Fig. 2 Surface pressure vs axial distance for Mach 6 at $\alpha = 8$ deg.

The center of pressure comparisons are shown in Fig. 3. Results from both methods showed very good agreement with experimental data for the normal force and pitching moment coefficient. The center of pressure comparisons are in fairly good agreement, but disagreement is noted for angles of attack less than 2 deg. It was conjectured that the disagreement between theory and experiment for x_{cp} at low angle of attack might be due to an inaccurate estimate of the wind tunnel model's wall temperature. For example, force and moment measurements could have been initiated at low angle of attack with the model relatively cold. As the pitch sweep proceeded, the model heated up and approached a temperature nearer the value used in the theoretical calculations. (The wall temperature values used for all of the calculations in this paper were obtained from the references quoted or from individuals familiar with testing procedures in the wind tunnel involved.) This conjecture for the disagreement, however, was discarded when calculations for relatively cold wall conditions produced changes in x_{cp} less than 0.002L at $M_\infty = 5.95$.

Mach 10 Comparisons

In Figs 4 and 5, the center of pressure and axial force are compared for Mach 10.1, and a Reynolds number of 2.9 million, for which laminar 3DV and PNS solutions were obtained. The cone half-angle of this model was 4 deg with a 0.125 in. nose diameter, and a length of 17.04 in. The center of pressure prediction from the 3DV codes is consistently 1% low over the angle of attack range, whereas the PNS code is somewhat higher. Both methods show fair agreement with forebody axial force over the angle of attack range. The 3DV code results agree very well with the axial force at zero angle of attack. It does not, however, show the proper increase in axial force with angle of attack. The PNS predictions are approximately 10% higher at zero angle of attack, but show good agreement for angles of attack above one deg. Possibly explaining the disagreement, it has been found from numerical experiments that the axial force coefficient can vary 10% depending on the wall temperatures used in the simulation.

Figure 6 shows the results for surface pressure comparisons at Mach 9.82, and Reynolds number of 0.459

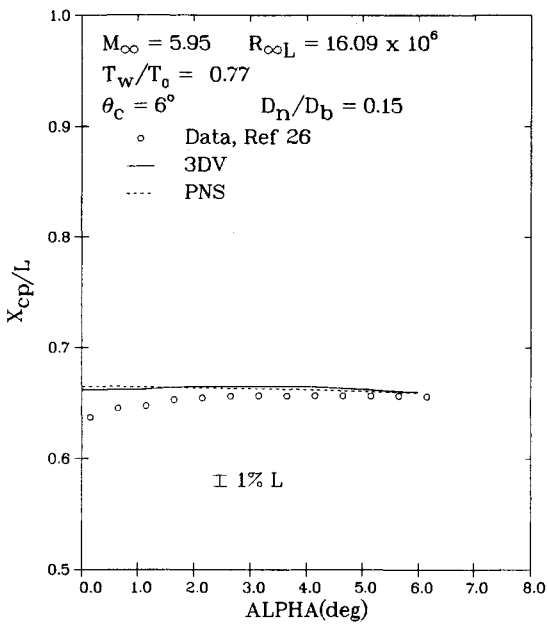

Fig. 3 Center of pressure vs angle of attack for Mach 6.

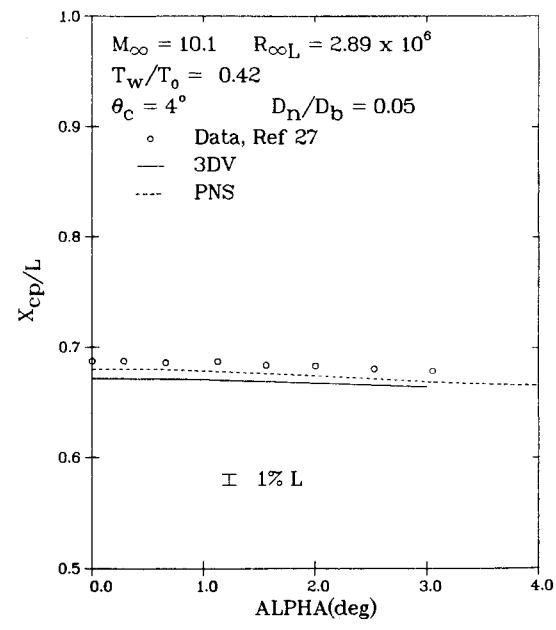

Fig. 4 Center of pressure vs angle of attack for Mach 10 high R_{∞_L}.

million. This model also had a 4 deg cone half-angle; however, the nose diameter was 0.56 in., and the length was 14.13 in. The pressure comparison is at an angle of attack of 2.97 deg and a laminar boundary layer was assumed for the 3DV and PNS solutions. The figure shows the axial distribution of surface pressure for the windward and leeward sides. The PNS code results are in good agreement with the data. The 3DV code results show better agreement on the windward side than on the leeward. This is due to the thin boundary layer on the windward side. The leeward side is a region of strong viscous-inviscid interaction where the inviscid/boundary layer solution may not yield an acceptable solution. The 3DV results for the windward meridian show distinct "wiggles" or roughness in the axial variation of surface pressure. This roughness is not seen in the inviscid distribution and is a result of the induced pressure increment calculated by the boundary-layer code. The 3DV code utilizes an entropy layer swallowing technique to find the boundary-layer edge conditions. It is believed that the "wiggles" appearing in the boundary-layer characteristics and, therefore, in the induced pressure increment, are caused by inaccuracies in this entropy layer swallowing technique.

Figures 7 and 8 show the comparisons for center of pressure and axial force for Mach 9.81, with a Reynolds number of 0.43 million. The cone half-angle of this model was 4 deg with a 0.125-in. nose diameter, and a length of 17.041 inches. The PNS code results showed good agreement with normal force and pitch moment data, while the 3DV code slightly overpredicts these quantities. For center of pressure, however, both solutions are consistently lower than the data. In the axial force comparison, the PNS results show excellent agreement with the data, but the 3DV results

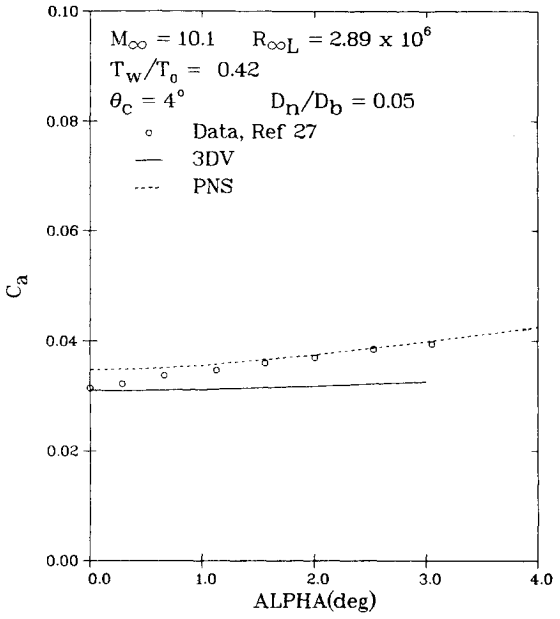

Fig. 5 Axial force vs angle of attack for Mach 10 high R_{∞_L}.

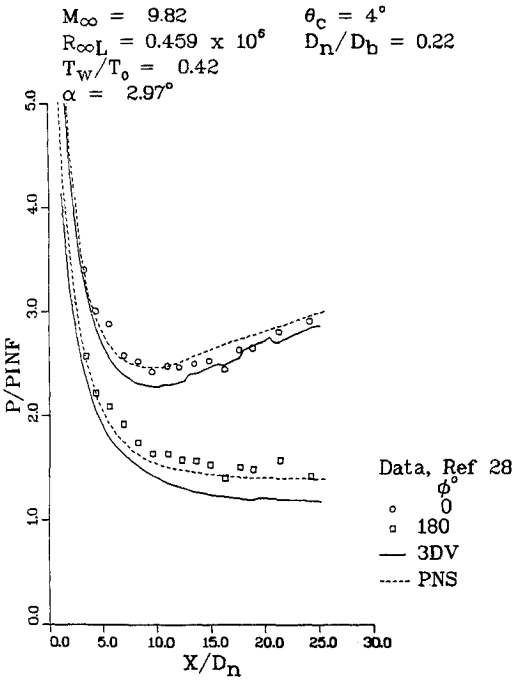

Fig. 6 Surface pressure vs axial distance for Mach 10 at $\alpha = 3$ deg.

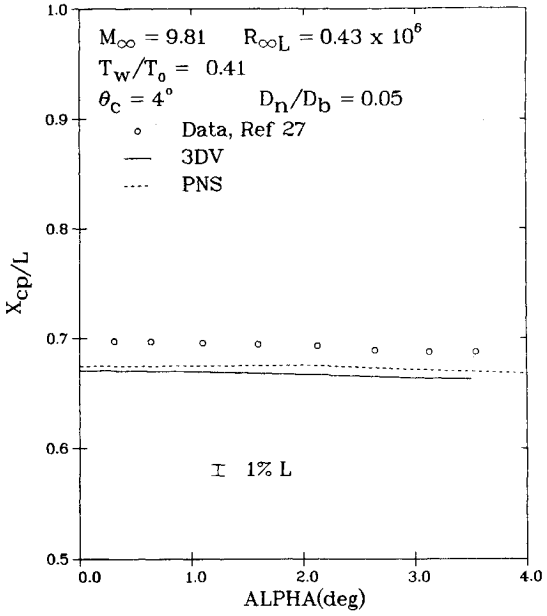

Fig. 7 Center of pressure vs angle of attack for Mach 10 low R_{∞_L}.

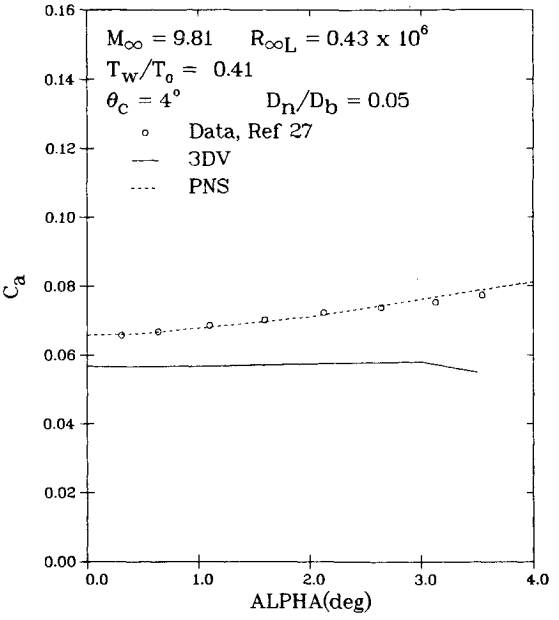

Fig. 8 Axial force vs angle of attack for Mach 10 low R_{∞_L}.

are considerably lower. As the Reynolds number is six times lower than in the previous axial force comparison, one would expect the larger disagreement between 3DV and experimental data shown in Fig. 8.

The reason for the significantly lower 3DV prediction of axial force at low Reynolds numbers can be understood by examining the surface pressure. The PNS code is predicting higher values of surface pressure because of the strong coupling between the inviscid outer flow an the viscous boundary-layer flow. The assumption of weak viscous interaction, used in the boundary-layer approach, is faulty for two primary reasons. First, the inviscid flow is moved outward due to the boundary-layer displacement thickness. This causes a larger flow turning angle, particularly on the leeside, and thus a higher surface pressure. Second, the edge conditions for the boundary-layer solution are taken as those on the surface of the body. As the boundary-layer thickness becomes significant compared to the shock layer thickness, the edge conditions become seriously in error. The difference between PNS and 3DV predictions should increase as the amount of viscious-inviscid interaction increases.

Mach 14 Comparisons

The comparisons of surface pressure for Mach 14.2, a Reynolds number of 0.72 million, and an angle of attack of 2 deg are shown in Fig. 9. This model had a 5.6-deg cone half-angle with a 0.3-in. nose diameter and a length of 13.91 in. The 3DV and PNS solutions were obtained assuming a laminar boundary layer. For the zero angle of attack case, the PNS code agreed fairly well with the experimental data. The 3DV code, however, was predicting lower values of pressure, as expected.

In Figs. 10 and 11, results are presented for the center of pressure and axial force coefficients for a Reynolds number of 0.57 million and Mach number of 14.3. This model had a 7-deg cone half-angle with a 0.3-in. nose diameter and a length of 11.14 in. Both methods show good agreement for the normal force, pitch moment, and the center of pressure. As expected, the 3DV code predicts a smaller axial force than the PNS code. The 3DV results, however, are in better agreement with the experimental data. This result was unexpected because of the excellent agreement of the PNS calculation with the axial force data for Mach 9.81 and at a slightly lower Reynolds number.

The results shown in Figs. 10 and 11 are for much higher angles of attack than seen previously. There were no PNS predictions obtained above the angle of attack of 14 deg because of the difficulties encountered in obtaining PNS solutions for these high angles of attack. It should be possible to obtain solutions for higher angles of attack, but one must have time and patience to use different input parameters until a solution can be obtained. After attempting several solutions for angles of attack greater than 14 deg, they were not pursued further for this paper. It should be noted that the 3DV solutions were obtained up to a 25-deg angle of attack with no difficulties.

Figure 12 shows results at Mach 14.1 for a Reynolds number of 15.2 million. For this high Reynolds number, a

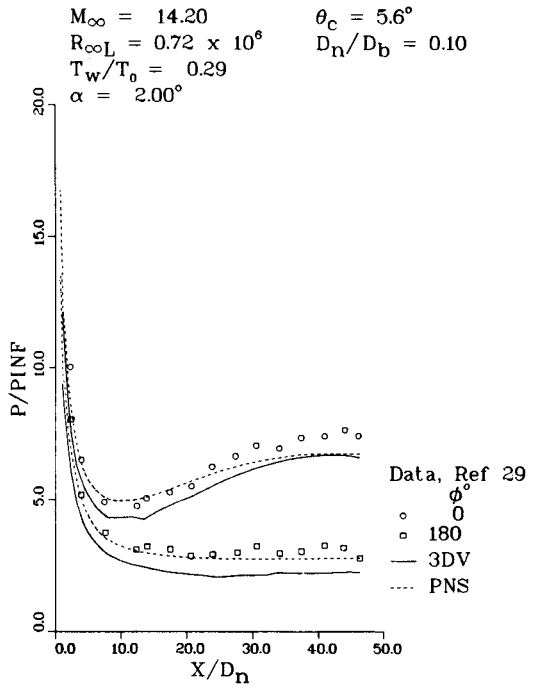

Fig. 9 Surface pressure vs axial distance for Mach 14 at $\alpha = 2$ deg, low R_{∞_L}.

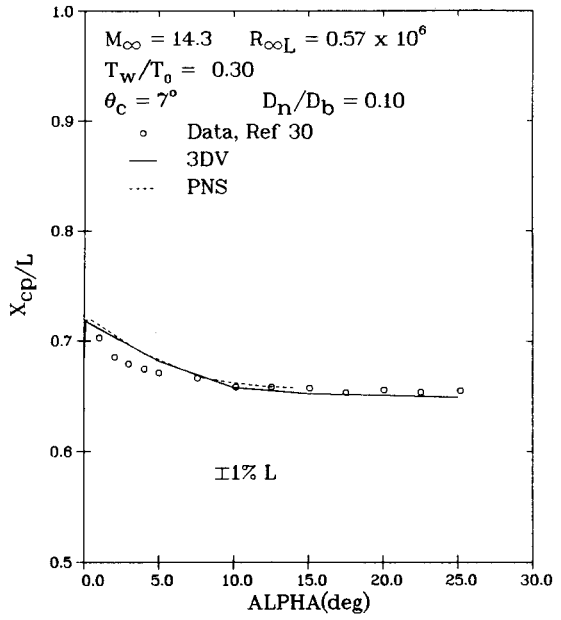

Fig. 10 Center of pressure vs angle of attack for Mach 14.

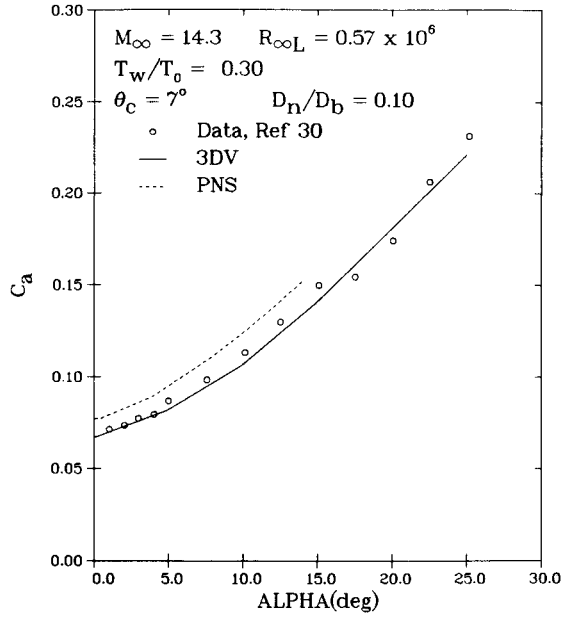

Fig. 11 Axial force vs angle of attack for Mach 14.

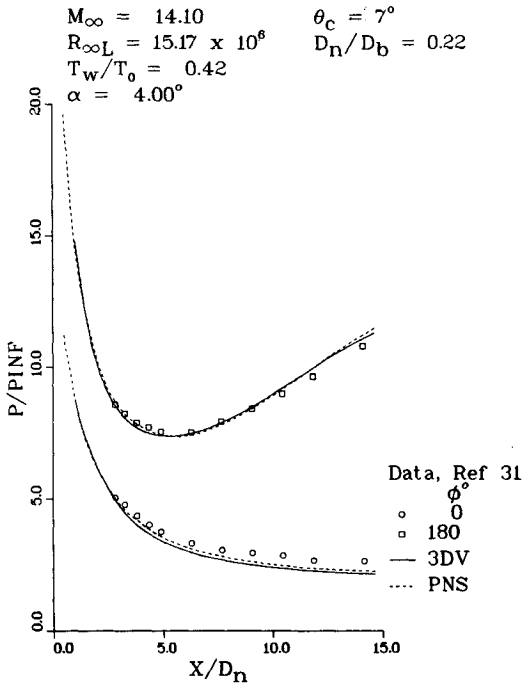

Fig. 12 Surface pressure vs axial distance for Mach 14 at $\alpha = 4$ deg, high R_{∞_L}.

turbulent boundary layer was assumed for the PNS and 3DV solutions. The sphere-cone model had a 7 deg half-angle with a 3.6-in. diameter nose and a length of 52.75 in. Comparisons are provided for the surface along the windward and leeward sides of the cone at an angle of attack of 4 deg. The predictions of both codes are in very good agreement with the data. This comparison demonstrates that excellent boundary-layer predictions for surface pressure can be obtained at the higher Mach number, but the Reynolds number must also be correspondingly higher.

Range of Applicability of Approaches

From the aforementioned pressure and force and moment comparisons, one can suggest a range of applicability of the two numerical approaches. The PNS approach compared well with both the pressure and force and moment data over the range of Mach and Reynolds number, except certain Mach 14 pressure data. The inviscid/boundary-layer approach, however, yielded good results for certain combinations of Mach and Reynolds numbers. As pointed out earlier, viscous interaction with the inviscid flow accounts for the disagreement.

One parameter which might aid in determining the range of applicability of the inviscid/boundary-layer technique is the hypersonic viscous interaction parameter $\bar{v}_\infty$. For bodies of revolution, it is defined by the following equation,[25]

$$\bar{v}_\infty = M_\infty (C_\infty / R_{\infty L})^{1/2}$$

where

$$C_\infty = (\mu_w/\mu_\infty)(T_\infty/T_w) \qquad (3)$$

where μ is viscosity, and T is temperature. As this parameter is based on slender bodies at zero incidence, it probably underpredicts the amount of viscous interaction at angle of attack. This is supported by both Figs. 5 and 8. At zero angle of attack the error due to viscous interaction is a minimum, but the error increases with angle of attack. This is due to the rapid growth of boundary-layer thickness on the leeside of the body.

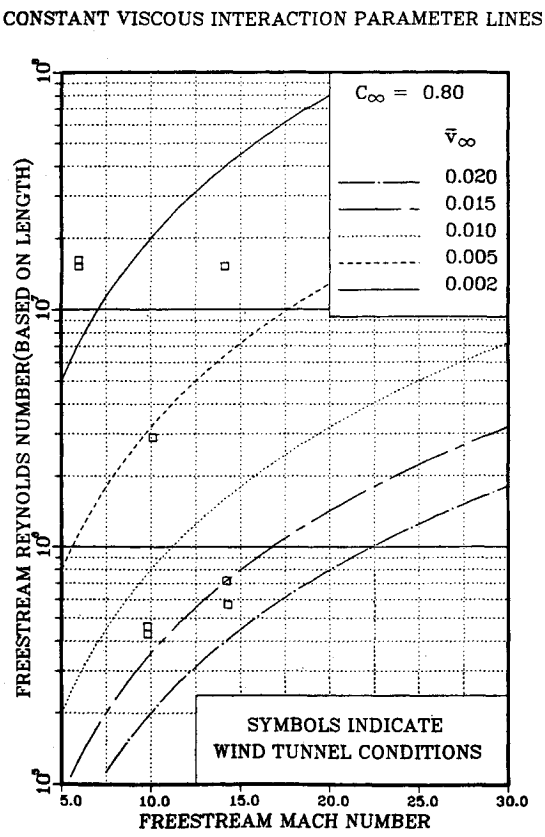

Fig. 13 Correlation of $\bar{v}_\infty$ with Mach number and Reynolds number.

Figure 13 shows the lines of constant $\bar{v}_\infty$ for the different combinations of Mach and Reynolds numbers. Also shown in the figure (as squares) are the Reynolds number and Mach number combinations used for both the pressure and force and moment comparisons. Using $\bar{v}_\infty$ as a means of correlating the viscous-inviscid interaction, the Mach 5.95 cases have the weakest interaction and the lower Reynolds number Mach 10 and 14 cases have the strongest interaction. The comparisons presented show that for $\bar{v}_\infty$ less than 0.0045 the inviscid/ boundary-layer solutions yield very good agreement with force and moment data, with the exception that the the drag-due-to-lift is slightly underpredicted. For $\bar{v}_\infty = 0.015$ the normal force and pitch moment from the boundary layer method is slightly overpredicted while the zero-lift axial force is underpredicted by 15%. The earlier work of Whitfield and Griffith[25] suggests good agreement between boundary-layer theory and experimental data for slender cones up to $\bar{v}_\infty = 0.1$. The present results clearly show that the zero-lift drag coefficient predicted by boundary-layer theory begins to deviate from experiment at $\bar{v}_\infty = 0.015$.

An additional consideration is the possible effect of cone bluntness on the just quoted values of $\bar{v}_\infty$. The present comparisons with experiment range from a nose bluntness of 0.05 up to .22. How the suggested values of $\bar{v}_\infty$ are affected by nose bluntness ratio has not been investigated.

Concluding Remarks

The work presented herein attempts to provide an assessment of an inviscid/boundary-layer method and a PNS method by comparing both with experimentally measured surface pressures and forces and moments for spherically blunted slender cones. It was found that the inviscid/boundary layer solutions compared well with experimental data except for certain Mach 14 comparisons. The inconsistencies in

some comparisons appear to be due to inconsistencies in the wind tunnel data itself.

The viscous interaction parameter $\bar{v}_\infty$ was suggested as a possible correlation for Mach number and Reynolds number combinations for which the inviscid/boundary-layer technique will provide predictions with acceptable accuracy. It is suggested that the inviscid/boundary-layer solution be used for surface pressure and axial force predictions for values of $\bar{v}_\infty$ up to 0.005. The inviscid/boundary-layer solution should be used for prediction of normal force and pitch moment for values of $\bar{v}_\infty$ up to 0.015. The PNS approach should be used for predictions for surface pressure and forces and moments for values of $\bar{v}_\infty$ greater than those stated above. Although the PNS approach yielded accurate predictions for values of $\bar{v}_\infty$ less than those stated, the inviscid/boundary-layer approach is recommended because of the faster computing times and ease of use.

The degree of difficulty in obtaining an inviscid/boundary-layer and a PNS solution was discussed. The PNS solution generally requires a large amount of user interaction and the adjustment of various input parameters in order to obtain an accurate solution. The inviscid/boundary-layer solution is straightforward to obtain and is, thus, very well suited for a design environment where rapid job turnaround and low user interaction requirements are significant considerations. The user must balance the accuracy requirements with the computer time and user work requirements to obtain a solution. The work presented here should help in determining when the increased accuracy of the PNS solution justifies the additional work necessary to obtain that solution.

Acknowledgment

This work was performed at Sandia National Laboratories under U.S. Department of Energy contract DE-AC04-76-DP00789.

References

[1]Kutler, P., Reinhardt, W. A., and Warming, R. F., "Numerical Computation of Multishocked, Three-Dimensional Supersonic Flow Fields with Real Gas Effects," AIAA Paper 72-702, June 1972.

[2]Marconi, F., Yaeger, L., and Hamilton, H., "Computation of High Speed Inviscid Flows about Real Configurations," *Aerodynamic Analyses Requiring Advanced Computers,* Part II, NASA SP-347, March 1975.

[3]Kyriss, C. L. and Harris, T. B., "A Three Dimensional Flow Field Computer Program for Maneuvering and Ballistic Reentry Vehicles," Presented at the Tenth Navy Symposium on Aeroballistics, July 1975.

[4]Solomon, J. M., Ciment, M., Ferguson, R. E., and Bell, J. B., "Inviscid Flow Field Calculations for Re-entry Vehicles with Control Surfaces," *AIAA Journal,* Vol. 15, Dec. 1977, pp. 1742-1749.

[5]Daywitt, J. Brant, D., Bosworth, F., "Computational Technique for Three-Dimensional Inviscid Flow Fields about Re-entry Vehicles," U.S. Air Force, SAMSO TR-79-5, April 1978.

[6]DeJarnette, F. R. and Hamilton, H. H., "Aerodynamic Heating on 3-D Bodies Including the Effects of Entropy Layer Swallowing," AIAA Paper 74-602, June 1974.

[7]Hecht, A. M., and Nestler, D. E., "A Three-Dimensional Boundary Layer Computer Program for Sphere Cone Type Re-entry Vehicles," AFFDL TR-78-67, Vol. I, June 1978.

[8]Rudman, S. and Rubin, S. G., "Hypersonic Viscous Flow Over Slender Bodies Having Sharp Leading Edges," *AIAA Journal,* Vol. 7, Sept. 1969, pp. 1744-1751.

[9]Nardo, C. T., and Cresci, R. J., "An Alternating Directional Implicit Scheme for Three-Dimensional Hypersonic Flows," *Journal of Computational Physics,* Vol. 8, Oct. 1971, pp. 268-284.

[10]Lin, T. C. and Rubin, S. G., "Viscous Flow Over a Cone at Moderate Incidence: I. Hypersonic Tip Region," *Computers and Fluids,* Vol. 1, No. 1, 1973, pp. 37-57.

[11]Lubard, S. C. and Helliwell, W. S., "Calculation of the Flow on a Cone at High Angle of Attack," *AIAA Journal,* Vol. 12, July 1974, pp. 965-974.

[12]Pantankar, S. V. and Spalding, D. B., "A Calculation Procedure for Heat, Mass and Momentum Transfer in Three-Dimensional Parabolic Flows," *International Journal of Heat and Mass Transfer,* Vol. 15, Oct. 1972, pp. 1787-1806.

[13]McDonald, H. and Briley, W. R., "Three-Dimensional Supersonic Flow of a Viscous or Inviscid Gas," *Journal of Computational Physics,* Vol. 19, March 1975, pp. 150-178.

[14]Vigneron, Y. C., Rakich, J. V., and Tannehill, J. C., "Calculation of Supersonic Viscous Flow Over Delta Wings with Sharp Subsonic Leading Edges," AIAA Paper 78-1137, July 1978.

[15]Schiff, L. B. and Steger, J. L., "Numerical Simulation of Steady Supersonic Viscous Flow," NASA Technical Paper 1749, May 1981.

[16]Chaussee, D. S., Patterson, J. L., Kutler, P., Pulliam, T.H., and Steger, J.L., "A Numerical Simulation of Hypersonic Viscous Flows Over Arbitrary Geometries at High Angle of Attack," AIAA Paper 81-0050, Jan. 1981.

[17]Rizk, Y. M., Chaussee, D. S., and McRae, D. S., "Computation of Hypersonic Viscous Flow Around Three-Dimensional Bodies at High Angles of Attack," AIAA Paper 81-1261, June 1981.

[18]Nicolet, W. E., Shanks, S., and Srinivasan, G., "Flowfield Predictions About Lifting Entry Vehicles," AIAA Paper 82-0026, Jan. 1982.

[19]Shanks, S. P., Srinivasan, G. R., and Nicolet, W. E., "AFWAL Parabolized Navier-Stokes code: Formulation and User's Manual," AFWAL-TR-82-3034, June 1982.

[20]Taylor, T. D. and Masson, B. S., "Applications of the Unsteady Numerical Method of Godunov to Computational of Supersonic Flows Past Bell-Shaped Bodies," *Journal of Computational Physics,* Vol. 5, June 1970, pp. 443-454.

[21]Widhopf, G. F., and Victoria, K. J., "Numerical Solution of the Unsteady Navier-Stokes Equations for the Oscillatory Flow Over a Concave Body," *Lecture Notes in Physics, No. 35, Proceedings of the Fourth International Conference on Numerical Methods in Fluid Dynamics,* edited by R. D. Richtmyer, Boulder, CO, June 1974, pp. 431-444.

[22]Chaussee, D. S., Kutler, P., and Pulliam, T. H., "Three Dimensional Flow Field Program," Flow Simulations Incorporated Rept. 80-08, 1980.

[23]Baldwin, B. S., and Lomax, H., "Thin Layer Approximation and Algebraic Model for Separated Turbulent Flows," AIAA Paper 78-257, 1978.

[24]Rubin, S. G. and Lin, T. C., "Numerical Methods for Two- and Three-Dimensional Viscous Flow Problems: Application to Hypersonic Leading Edge Equations," Polytechnic Institute of Brooklyn Aeronautical Laboratories Rept. 71-8 (AFOSR-TR-71-0778), 1971.

[25]Whitfield, J. D. and Griffith, B. J., "Hypersonic Viscous Drag Effects on Blunt Slender Cones," *AIAA Journal,* Vol. 2, No. 10, 1964, pp. 1714-1722.

[26]Stone, G. W., Unpublished data, 1975. See also: Baker, S. S., "Static Stability and Pressure Distribution Tests of a Slender Cone Model With Symmetric and Asymmetric Nosetips at Mach Number 6," AEDC-TR-75-56, 1975.

[27]Griffith, B. J., Strike, W. T., and Majors, B. M., "Ablation and Viscous Effects on the Force and Moment Characteristics of Slender Cone Models at Mach 10 Under Laminar Flow Conditions," AEDC-TR-75-109, 1975.

[28]Boylan, D. E., Strike, W. T., and Shope, F. L., "A Direct Comparison of Analytical and Experimental Surface and Flow-Field Data on a 4-deg. Cone at Incidence in a Hypersonic Stream With Laminar Boundary Layers," AEDC-TR-76-84, 1976.

[29]Stetson, K. F., "Experimental Results of Laminar Boundary Layer Separation on a Slender Cone at Angle of Attack at Mach 14.2," U.S. Air Force Aerospace Research Laboratories Rept. 71-0127, 1971.

[30]Scaggs, N. E. and Gillies, D. S., "Aerodynamic Characteristics of Biconic Configurations at Mach 14," AFWAL/FIMG, Wright-Patterson AFB, 1981.

[31]Prats, B. D., unpublished data, Naval Surface Weapons Center, White Oak, Tunnel 9.

[32]Rubin, S. G., "A Review of Marching Procedures For Parabolized Navier-Stokes Equations," Presented at Symposium on Numerical and Physical Aspects of Aerodynamic Flows, California State University, Long Beach, CA, Jan. 1981.

[33]McWherter, M., Noack, R. W., and Oberkampf, W. L., "Evaluation of Inviscid/Boundary Layer and Parabolized Navier-Stokes Solutions for Design of Re-entry Vehicles," AIAA Paper 84-0486, 1984.